Variational nature of the frozen density energy in density-based energy decomposition analysis and its application to torsional potentials

Qin Wu

Citation: The Journal of Chemical Physics **140**, 244109 (2014); doi: 10.1063/1.4884961
View online: http://dx.doi.org/10.1063/1.4884961
View Table of Contents: http://aip.scitation.org/toc/jcp/140/24
Published by the American Institute of Physics

Variational nature of the frozen density energy in density-based energy decomposition analysis and its application to torsional potentials

Qin Wu[a)]
Center for Functional Nanomaterials, Brookhaven National Laboratory, Upton, New York 11973, USA

(Received 15 April 2014; accepted 12 June 2014; published online 27 June 2014)

The density-based energy decomposition analysis (DEDA) is the first of its kind to calculate the frozen density energy variationally. Defined with the constrained search formulation of density functional theory, the frozen density energy is optimized in practice using the Wu-Yang (WY) method for constrained minimizations. This variational nature of the frozen density energy, a possible reason behind some novel findings of DEDA, will be fully investigated in this work. In particular, we systematically study the dual basis set dependence in WY: the potential basis set used to expand the Lagrangian multiplier function and the regular orbital basis set. We explain how the convergence progresses differently on these basis sets and how an apparent basis-set independence is achieved. We then explore a new development of DEDA in frozen energy calculations of the ethane molecule, focusing on the internal rotation around the carbon-carbon bond and the energy differences between staggered and eclipsed conformations. We argue that the frozen density energy change at fixed bond lengths and bond angles is purely steric effects. Our results show that the frozen density energy profile follows closely that of the total energy when the dihedral angle is the only varying geometry parameter. We can further analyze the contributions from electrostatics and Pauli repulsions. These results lead to a meaningful DEDA of the torsional potential in ethane. © *2014 AIP Publishing LLC*. [http://dx.doi.org/10.1063/1.4884961]

I. INTRODUCTION

One of the most unique features in the density-based energy decomposition analysis (DEDA)[1] is its calculation of the frozen density energy. In analyzing the total interaction energy between two molecules (or fragments) that form a complex, it is customary to ask what the energy would be if two infinitely separated molecule are brought together without relaxing their electron densities. In wave function-based energy decomposition analysis (EDA), such step is achieved by forming a properly antisymmetrized supermolecule wave function from unrelaxed molecular orbitals (MO) of each fragments, such as the Heitler-London wave function. However, because MOs from different fragments are nonorthogonal, the electron density corresponding to this antisymmetrized wave function is not a sum of the fragment electron densities. This change in the "frozen density" creates a difficulty in separating the electrostatic term from the Pauli repulsion term that is meant to be covered by the antisymmetrization. Therefore, this energy is sometimes called Heitler-London energy instead of frozen density energy.[2,3] With a density-base approach, DEDA overcomes this problem by focusing on antisymmetric supermolecule wave functions (e.g., Slater determinants) that actually reproduce the frozen density. Hence only the densities from individual fragments are used, not the MOs. Moreover, because of the many-to-one mapping between wave functions and the density, DEDA searches for the one that gives the lowest total energy. As results, the frozen density energy in DEDA not only provides a meaningful separation between the electrostatics and the Pauli repulsion terms, but also is variational.

Like other supermolecule EDA methods,[4–14] DEDA uses energies of intermediate states to break down the total binding energy into frozen density energy, polarization energy and charge transfer energy (In this work, we will not consider geometry distortion of fragments and the binding energy is basis-set superposition error (BSSE) corrected.):

$$\Delta E_{\text{bind}} = \Delta E_{\text{frz}} + \Delta E_{\text{pol}} + \Delta E_{\text{ct}}. \quad (1)$$

DEDA differs, however, in that all the intermediate energies are variationally determined. The significance of a variational intermediate state has been discussed in the context of polarization and charge transfer, where optimal charge localized states as achieved in the block localized wave function (BLW)-EDA[2,3,15,16] and later the absolutely localized MO (ALMO)-EDA[17,18] are considered the key to avoiding overestimation of the charge transfer term. In DEDA the energy of the state before charge transfer is also variationally calculated, where we use constrained density functional theory (DFT).[19] Our results confirm the small contribution from charge transfer in the hydrogen bonding.[1] On the other hand, a variational frozen density energy has only become available with DEDA; hence its significance is much less discussed. Our early results show that the frozen density energy in DEDA reproduces the angle and distance dependence of the hydrogen bond very well.[19] While its implication to the understanding of chemical bonds is yet unclear, these results are found to be useful for force field development.[20,21] To facilitate future discussion on the frozen density energy, our first goal of this work is to elaborate its variational nature.

a)Electronic mail: qinwu@bnl.gov

The second goal of this work is to extend DEDA into intramolecular interactions. Because the frozen density energy can be defined for fragments that are not closed-shell molecules, DEDA in theory can be applied to interactions between different parts of the same molecule. The complication here is that when such fragments form a molecule, their interactions can be both bonded and nonbonded, even at the frozen density level. It will be quite a challenge to unravel the bonded interactions from nonbonded ones in the frozen density energy. However, there are situations where bonded interactions can be viewed as constant, so the change in the frozen density energy reflects purely the change in nonbonded interactions. Such is exactly what one may expect for the internal rotation around a single bond, i.e., a torsional potential. We will perform an initial test of this idea and show that the frozen density energy profile of the torsion indeed provides a meaningful decomposition of the rotational barrier.

For the rest of this work, in Sec. II we will first review the constrained search formulation of the frozen density energy and the Wu-Yang (WY) method[22] that we use for its practical calculation. Our emphasis is on its variational nature in the unconstrained maximization of WY, in particular its dependence on the potential basis set. The relationship between the potential basis set and the orbital basis set will be thoroughly discussed in Sec. III, supported by numerical results from the neon dimer. We will then turn to frozen density energy calculations of the ethane molecule in Sec. IV, study in detail the difference between its staggered and eclipsed conformations, and finally present a torsional potential profile from the frozen density energy perspective.

II. FROZEN DENSITY ENERGY FROM THE CONSTRAINED SEARCH

Our definition of the frozen density energy is built on the constrained search formulation of DFT,[23] which was pioneered by Levy[24] to augment the Hohenberg-Kohn theorems.[25] We are, however, concerned with practical calculations in the Kohn-Sham scheme[26] with an approximate energy functional $E[\rho(\mathbf{r})]$. In Kohn-Sham (KS), ρ is built from a single Slater determinant, and $E[\rho]$ is a partially implicit functional of ρ because the kinetic energy and possibly some exchange energy (as in hybrid functionals) are directly calculated from orbitals. We define the energy of a given density ρ_f, i.e., the frozen density energy, as

$$\mathsf{E}[\rho_f(\mathbf{r})] = \min_{\rho\to\rho_f} E[\rho(\mathbf{r})]. \tag{2}$$

The constraint $\rho \to \rho_f$ is understood as searching over all Slater determinants that have the same density as ρ_f. Obviously $\mathsf{E}[\rho_f(\mathbf{r})] \geq E_0$ where E_0 is the ground state energy of the complex. The frozen density energy consequently serves as a meaningful intermediate state to decompose the total interaction energy.

The definition of $\mathsf{E}[\rho_f(\mathbf{r})]$ is equally valid within any particular Kohn-Sham DFT model, consisting of an approximate exchange-correlation functional, a basis set to expand molecular orbitals, and an integration grid. To compute $\mathsf{E}[\rho_f(\mathbf{r})]$ practically we use the Wu-Yang method[22] to carry out the constrained minimization in Eq. (2). In WY, a new functional, i.e., the Lagrangian, is defined with the help of a Lagrangian multiplier function $v_\lambda(\mathbf{r})$.

$$W_s[\rho, v_\lambda(\mathbf{r})] = E[\rho(\mathbf{r})] + \int v_\lambda(\mathbf{r})\{\rho(\mathbf{r}) - \rho_f(\mathbf{r})\}d\mathbf{r}. \tag{3}$$

WY continue to show that W_s can be turned into a concave functional of $v_\lambda(\mathbf{r})$, and the constrained minimization is then transformed into an unconstrained maximization, a relatively easier problem to solve. In mathematic optimization, the WY method can be viewed as a primal-dual method[27] where the dual functional is defined as

$$W_d[v_\lambda(\mathbf{r})] = \min_\rho \left(E[\rho] + \int v_\lambda(\mathbf{r})\{\rho(\mathbf{r}) - \rho_f(\mathbf{r})\}d\mathbf{r} \right).$$

The Lagrange duality guarantees that $W_d[v_\lambda(\mathbf{r})] \leq \mathsf{E}[\rho_f(\mathbf{r})]$.[27] In another words,

$$\mathsf{E}[\rho_f(\mathbf{r})] = \min_{\rho\to\rho_f} E[\rho(\mathbf{r})] = \max_{v_\lambda} W_d[v_\lambda(\mathbf{r})]. \tag{4}$$

Note that the second equality holds only for the optimal $v_\lambda(\mathbf{r})$, which is unfortunately very hard to compute. In order to solve $v_\lambda(\mathbf{r})$ more efficiently, WY uses a basis set expansion $v_\lambda(\mathbf{r}) = \sum_t b_t g_t(\mathbf{r})$, where the basis functions $g_t(\mathbf{r})$ are conveniently chosen to be atom-centered gaussians. We call this new basis set potential basis set (PBS) because it becomes part of the Kohn-Sham potential that determines the KS orbitals. PBS does not have to be the same as the orbital basis set (OBS). Once both OBS and PBS are chosen, the optimization is then turned into solving for the expansion coefficients b_t to maximize W_d, which can be done efficiently because both the first and second derivatives are available.[22]

In DEDA, we use the optimized W_d with a given PBS as the frozen density energy E_{frz}. It can be concluded from the above discussion that E_{frz} is a lower bound of the exact $\mathsf{E}[\rho_f(\mathbf{r})]$ for a given model. Therefore, within the model, the variational nature of E_{frz} has at least a two-fold meaning: it is determined variationally for a given potential basis set and it has a complete potential basis set limit. The second point is important when we study the quality a PBS. DEDA further defines the difference between E_{frz} and the sum of fragment energies as the frozen density contribution of the total interaction energy ($\Delta E_{\text{frz}} = E_{\text{frz}} - \sum E_{\text{fragment}}$); hence ΔE_{frz} also approaches its limit from below when we increase the PBS quality.

To explore the limit of ΔE_{frz}, it is worthwhile to examine the relation between E_{frz} and $\mathsf{E}[\rho_f(\mathbf{r})]$. $\mathsf{E}[\rho_f(\mathbf{r})]$ is defined under the condition $\rho(\mathbf{r}) - \rho_f(\mathbf{r}) = 0$, which has to be true for every $\mathbf{r}$. We call it the strong density constraint. On the other hand, E_{frz} is defined on a set of more feasible conditions,

$$\int \{\rho(\mathbf{r}) - \rho_f(\mathbf{r})\}g_t(\mathbf{r})d\mathbf{r} = 0, \tag{5}$$

for every $g_t(\mathbf{r})$ in the PBS. If $g_t(\mathbf{r})$ form a complete set, Eq. (5) is equivalent to the strong density constraint. However, the PBS in practice is never complete. With the atomic-centered gaussians we use, it is not clear how the completeness is approached. Although we can generally infer that increasing basis set size leads to better results, we need a separate measure that can be used to quantify how strong the

TABLE I. ΔE_{frz} and ϵ_ρ with different OBS and PBS combinations for the neon dimer. The unit for ΔE_{frz} is kcal/mol. ϵ_ρ is in term of number of electrons.

R			PBS					
(bohr)	OBS		D	aug-D	T	aug-T	Q	aug-Q
	aug-cc	ΔE_{frz}	64.35	66.54	66.66	69.34	71.28	72.28
	-pVDZ	ϵ_ρ	0.1328	0.0770	0.0731	0.0217	0.0076	0.0039
3.0	aug-cc	ΔE_{frz}	62.75	64.48	64.95	65.73	65.96	66.83
	-pVTZ	ϵ_ρ	0.1501	0.0940	0.0664	0.0411	0.0356	0.0045
	aug-cc	ΔE_{frz}	62.54	64.18	64.37	65.02	65.08	65.43
	-pVQZ	ϵ_ρ	0.1493	0.0929	0.0739	0.0404	0.0382	0.0160
	aug-cc	ΔE_{frz}	4.92	5.17	5.30	5.38	5.76	5.76
	-pVDZ	ϵ_ρ	0.0284	0.0212	0.0096	0.0042	0.0016	0.0011
4.0	aug-cc	ΔE_{frz}	4.89	4.96	4.99	5.02	5.01	5.09
	-pVTZ	ϵ_ρ	0.0297	0.0197	0.0138	0.0108	0.0105	0.0025
	aug-cc	ΔE_{frz}	4.87	4.94	4.97	4.98	4.98	5.01
	-pVQZ	ϵ_ρ	0.0295	0.0187	0.0122	0.0094	0.0099	0.0044

original density constraint is satisfied for a given PBS. It is for this purpose that we employ the simple and oft-used[28,29] integrated absolute density error ϵ_ρ defined as

$$\epsilon_\rho = \int |\rho(\mathbf{r}) - \rho_f(\mathbf{r})| d\mathbf{r}, \tag{6}$$

where the absolute value has to be used because $\rho(\mathbf{r}) - \rho_f(\mathbf{r})$ integrates to zero.

In Secs. III and IV, we will use both ΔE_{frz} and ϵ_ρ to investigate the basis set dependence of the frozen density energy. In general, we expect that a better potential basis set will give larger ΔE_{frz} and smaller ϵ_ρ. We will attempt to find a quantitative relation between these two, which will allow us to extrapolate to the limit when $\epsilon_\rho = 0$. Furthermore, we will also examine the orbital basis set dependence and make a recommendation of the best OBS/PBS combination for frozen density energy calculations. Unless otherwise specified, all our calculations in this work are done using the B3LYP exchange-correlation functional[30–32] in a development version of NWChem 5.1.[33]

III. BASIS SET DEPENDENCE OF THE FROZEN DENSITY ENERGY

A. Neon dimer

We use the simple system of neon dimer for our basis set dependence study. The MP2/aug-cc-pVQZ optimized internuclear distance for Ne_2 is 6.0 bohrs. Because B3LYP does not include long range van der Waals interactions, we use two distances, 3.0 and 4.0 bohrs, where the interatomic interaction is expected to be repulsive, and therefore ΔE_{frz} to be positive. All results are collected in Table I with different combination of orbitals basis set and potential basis set. We use a shorthand notation for PBS where the cardinal number X (X = D, T, or Q) and aug-X stand for Dunning's cc-pVXZ basis set[34] and its augmented version,[35] respectively.

We have observed before that ΔE_{frz} follows the trend of ΔE_{bind} as the interfragment distances increases.[1] Table I again shows a dramatic drop of ΔE_{frz} as Ne-Ne distance increases from 3.0 to 4.0 bohrs, as expected from an exponential decay of short-range repulsion. A couple of other observations can be made about ϵ_ρ from Table I. The first thing is that ϵ_ρ is never zero as the original density constraint requires to be. This is a manifestation of the fact that Eq. (5), the actual constraints satisfied in WY, is a weaker condition than $\rho(\mathbf{r}) - \rho_f(\mathbf{r}) = 0$. However, for a given system and a given OBS, increasing the size of PBS does decrease ϵ_ρ. To have a more detailed look of how the density error changes with OBS, we plot $\rho(\mathbf{r}) - \rho_f(\mathbf{r})$ along the interatomic axis in Fig. 1, where three frozen density calculation results are presented. These calculations use the same OBS but different PBS. For each calculation, $\rho(\mathbf{r}) - \rho_f(\mathbf{r})$ has its largest amplitude around the nuclei, which can be understood as a result of the small integration volumes for those densities, hence their insignificant contribution to the energy and other optimization targets. Overall, $\rho(\mathbf{r}) - \rho_f(\mathbf{r})$ approaches zero as OBS goes from double zeta to quadruple zeta even though the change is not spatially uniform.

Table I further shows that as ϵ_ρ decreases, ΔE_{frz} increases correspondingly, which is exactly the maximization

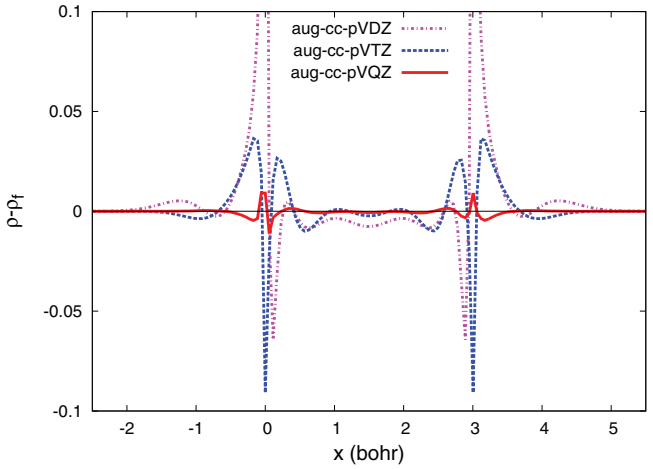

FIG. 1. $\rho(\mathbf{r}) - \rho_f(\mathbf{r})$ along the axis of the neon dimer for different PBS combination with the same OBS of aug-cc-pVTZ. Neon atoms are at x = 0 and x = 3.

TABLE II. The binding energy and the fitting parameters to Eq. (7) for the neon dimer. All numbers are in kcal/mol except for β, which is unitless.

R	OBS	ΔE_{bind}	ΔE^0_{frz}	α	β
	aug-cc-pVDZ	58.86	76.7	21.4	0.283
3.0	aug-cc-pVTZ	58.67	67.0	23.6	0.920
	aug-cc-pVQZ	58.58	65.6	33.3	1.28
	aug-cc-pVDZ	4.78	6.37	3.15	0.236
4.0	aug-cc-pVTZ	4.79	5.13	3.33	0.746
	aug-cc-pVQZ	4.78	5.03	6.98	1.08

process discussed in Sec. II. We will discuss the possibility of $\epsilon_\rho = 0$ in Sec. III B. For now, we assume the limit of zero ϵ_ρ exists and wish to find out what ΔE_{frz} might be at that limit. To do that, we examine Table I more closely and note that for the same OBS, when different PBS (such as aug-cc-pVDZ and cc-pVTZ) give nearly the same ϵ_ρ, ΔE_{frz} is also about the same. It suggests a quantitative relation between these two measures. After some trials, we find the following empirical formula gives a good representation:

$$\Delta E_{\text{frz}} = \Delta E^0_{\text{frz}} - \alpha \epsilon_\rho^\beta, \tag{7}$$

where ΔE^0_{frz} is the limit when $\epsilon_\rho = 0$, and both the prefactor α and exponent β control how fast the limit is approached. For each different OBS, we find the parameters (ΔE^0_{frz}, α and β) that best fit the data in Table I, with results listed in Table II. Next we plot ΔE^0_{frz} against ϵ_ρ in Fig. 2 with both the data and fitted lines. The fitting is generally very good except for maybe when aug-cc-pVDZ is the orbital basis set for $R = 4.0$.

Fig. 2 shows clearly the OBS dependence of ΔE^0_{frz}. To some degree, it is the same as regular DFT energies in that a better OBS leads to a lower frozen density energy at the zero ϵ_ρ limit. This OBS dependence is part of the variational nature of the frozen density energy, too. However, comparing ΔE_{bind} and ΔE^0_{frz} in Table II, we find significantly smaller changes in ΔE_{bind} than ΔE^0_{frz} among different OBS. More specifically, ΔE_{bind} appears to be already converged with aug-cc-pVDZ, while ΔE^0_{frz} can change by over 10% when aug-cc-pVQZ is used. On the other hand, Table I also shows that the OBS/PBS combination of aug-cc-pVDZ/cc-pVDZ gives about the same approximate ΔE_{frz} as aug-cc-pVQZ/cc-pVQZ, which was also observed in our earlier study of water dimer.[1] To understand these results better, we need to examine more closely the meaning of constrained search in a finite orbital basis set, which we will discuss next.

B. Constrained search in a finite orbital basis set

Our starting point to understand the variations in ΔE^0_{frz} is the finite orbital basis set and the linear dependencies among basis set products as pioneered by Harriman.[36,37] In DFT calculations with a finite basis set $\{\phi_\mu(\mathbf{r})\}$, the electron density is constructed by

$$\rho(\mathbf{r}) = \sum_{\mu\nu} P_{\mu\nu}\phi_\mu(\mathbf{r})\phi_\nu(\mathbf{r}), \tag{8}$$

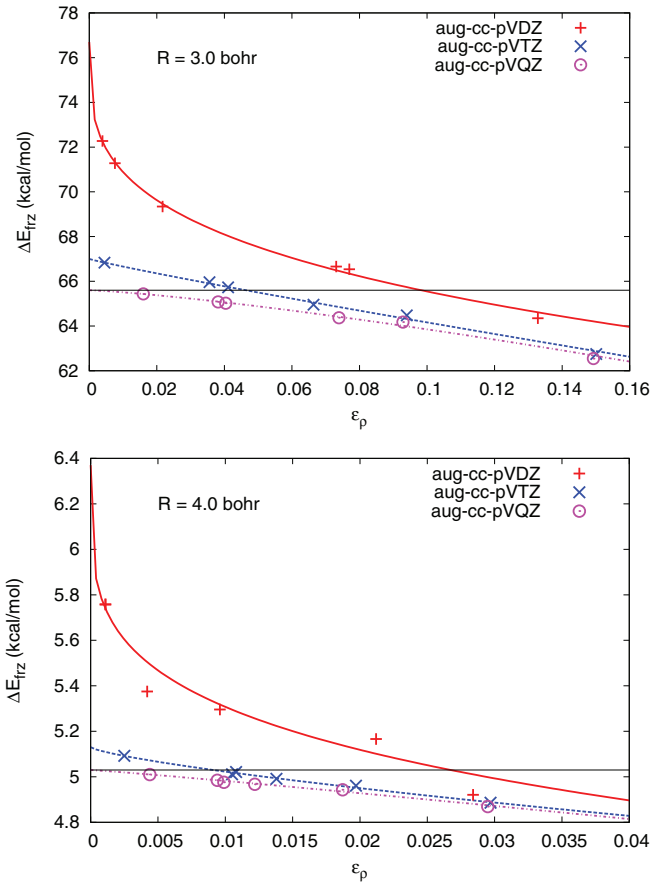

FIG. 2. ΔE_{frz} against ϵ_ρ for the neon dimer. The points are from data in Table I, while the lines are Eq. (7) with parameters from Table II, except for the thin black line, which represents ΔE^0_{frz} for aug-cc-pVQZ, using here as the OBS limit.

where the density matrix $P_{\mu\nu}$ is usually calculated from the molecular orbitals (ψ_i) which are linear combination of basis functions, $\psi_i = \sum_\mu C_{\mu i}\phi_\mu$,

$$P_{\mu\nu} = \sum_{i=1}^{N_e} C_{\mu i} C_{\nu i}, \tag{9}$$

and i goes through all occupied orbitals, which in KS scheme are the lowest N_e orbitals and N_e is the number of electrons. (We are only concerned with the total density with implicit spin summations.) The frozen density $\rho_f(\mathbf{r})$, instead, is built from the sum of fragment densities. Each fragment A is calculated in the full basis set of the whole system as in the Boys-Bernardi counterpoise correction.[38] Therefore, its density can be written in the same format as in Eq. (8). The frozen density is then

$$\begin{aligned}\rho_f(\mathbf{r}) &= \sum_A \sum_{\mu\nu} P^A_{\mu\nu}\phi_\mu(\mathbf{r})\phi_\nu(\mathbf{r}) = \sum_{\mu\nu}\sum_A P^A_{\mu\nu}\phi_\mu(\mathbf{r})\phi_\nu(\mathbf{r}) \\ &= \sum_{\mu\nu} P^f_{\mu\nu}\phi_\mu(\mathbf{r})\phi_\nu(\mathbf{r}),\end{aligned} \tag{10}$$

where $P^f_{\mu\nu} = \sum_A P^A_{\mu\nu}$. From Eqs. (8) and (10), the density constraint $\rho(\mathbf{r}) - \rho^f(\mathbf{r}) = 0$ becomes

$$\sum_{\mu\nu}(P_{\mu\nu} - P^f_{\mu\nu})\phi_\mu(\mathbf{r})\phi_\nu(\mathbf{r}) = 0. \tag{11}$$

TABLE III. Numbers of basis functions (N), basis function products ($N(N+1)/2$), eigenvalues of product overlap matrices smaller than a threshold θ. Cartesian basis functions for d and f types are used. When there are two numbers in a box, the one before is for $R = 3.0$ bohr of the neon dimer, followed by that for $R = 4.0$ bohrs.

Basis set	Types	No. func.	No. prod.	$\theta = 10^{-14}$	$\theta = 10^{-13}$	$\theta = 10^{-12}$
aug-cc-pVDZ	4*s*3*p*2*d*	50	1275	292/275	306/293	336/310
aug-cc-pVTZ	5*s*4*p*3*d*2*f*	110	6105	3396/3282	3699/3578	3835/3719

The trivial solution to Eq. (11), $P_{\mu\nu} - P^f_{\mu\nu} = 0$ for all $\mu\nu$, is not possible because the matrix $P_{\mu\nu}$ as built from Eq. (9) satisfies idempotency, while $P^f_{\mu\nu}$ does not. Therefore, a necessary condition for solutions to Eq. (11) is that there has to be linear dependency in the space of basis function products $\phi_\mu(\mathbf{r})\phi_\nu(\mathbf{r})$.

The linearly dependent products of basis functions were first studied by Harriman[36,37] and have been recently re-examined by Görling in the context of optimized effective potential.[39] They have shown that such linear dependency is guaranteed in a complete basis set. For finite basis sets, it is possible that such linear dependency does not exist in extreme cases.[28] However, Harriman and co-workers[37,40] have shown that near linear dependency occurs very quickly as the basis set size grows, and in the case of gaussians, is almost always present in practical calculations. Numerically, linear dependency is revealed from near zero eigenvalues of the product overlap matrix. In Table III we compare the number of linear dependencies in the basis function products of aug-cc-pVDZ and aug-cc-pVTZ for the neon dimer by comparing the number of eigenvalues of the product overlap matrix that are smaller than a threshold value. The aug-cc-pVDZ basis set has 4*s*3*p*2*d* contracted gaussian functions for a neon atom, while aug-cc-pVTZ has 5*s*4*p*3*d*2*f*. In terms of total number of basis functions (N), the latter has more that doubled the former. In terms of the total number of basis function products, the factor of difference is almost 5 because there are $N(N+1)/2$ unique basis function products. When the eigenvalues of the normalized product overlap matrix are examined, the number of those that can be considered zero (i.e., smaller than a threshold θ) is over 10 times more in aug-cc-pVTZ than in aug-cc-pVDZ. This increase of linear dependencies in basis function products provides more degrees of freedom in the variational search of the lowest energy state that reproduces the frozen density, and therefore leads to lower frozen density energy, just like what the increase of basis function does to DFT energies. However, most basis sets are designed to efficiently calculate ground state energies, which in combination with the different growth rates for the linear dependencies in basis function products and the basis functions themselves, are the reasons behind the difference in ΔE_{bind} and ΔE^0_{frz} in Table II.

C. Choosing the ΔE_{frz} in DEDA

The quantitative understanding of the potential basis set dependence of ΔE_{frz} has allowed us to extrapolate to its complete PBS limit, ΔE^0_{frz}, for a given orbital basis set. It may be natural to conclude that ΔE^0_{frz} should be used when the energy decomposition analysis is done in a given OBS. However, using ΔE^0_{frz} can present serious problems because the OBS convergence behavior is very different between ΔE_{bind} and ΔE^0_{frz}. Commonly used basis sets are optimized for ground state energies and properties. Therefore, when we go from aug-cc-pVDZ to aug-cc-pVQZ, the binding energy changes merely 0.3 kcal/mol (at $R = 3.0$ bohrs, even less at $R = 4.0$ bohrs). On the other hand, the frozen density energy calculations make use of the linear dependencies in the space of orbital basis function products, whose convergence is much less clear. Indeed, ΔE^0_{frz} decreases by over 10 kcal/mol from the smallest to the largest OBS. We can reasonably assume that the aug-cc-pVQZ result of ΔE^0_{frz} is close to its OBS limit. Therefore, if we use ΔE^0_{frz} of the aug-cc-pVDZ, we will have an error of 11.1 kcal/mol, which is unacceptable.

We are thus facing a practical issue where aug-cc-pVDZ already gives a good approximation to the OBS limit of the binding energy, but not to the OBS limit of ΔE^0_{frz}. Although one can always increase the orbital basis set to find the limit of ΔE^0_{frz}, it is time consuming and, we would argue, unnecessary. Indeed, we can get a good approximation of the OBS limit of ΔE^0_{frz} with a finite size PBS. Table I shows that the OBS/PBS combinations of aug-cc-pVXZ/cc-pVXZ for X = D, T, and Q all give small errors in ΔE_{frz} as compared to ΔE^0_{frz} of aug-cc-pVQZ. This seems to result from a balance of two factors: a smaller OBS has a larger ΔE^0_{frz} while for a given OBS a smaller PBS gives a smaller approximate ΔE_{frz}. Similar results were also seen in our previous study of water dimer,[1] where we noted the small basis set dependence of ΔE_{frz} when we used the OBS/PBS combinations of aug-cc-pVXZ/cc-pVXZ (X = D, T, and Q). Fig. 2 further illustrates this point with a thin horizontal line, corresponding to ΔE^0_{frz} of aug-cc-pVQZ, that crosses the aug-cc-pVTZ and aug-cc-pVDZ curves at increasing ϵ_ρ values. Therefore in practice, when a given OBS is chosen for DEDA, the frozen density energy calculation should be done with a PBS that is the same or slightly smaller than the OBS. Overall, we find that the best approximation to ΔE^0_{frz} of aug-cc-pVQZ is ΔE_{frz} from the OBS/PBS combination of aug-cc-pVTZ/aug-cc-pVTZ. We thus recommend this choice for frozen density energy calculations when affordable.

To further test our recommendation, we have performed calculations on selected systems from the A24 data set of noncovalent complexes.[41] We did not use the full data set because many of these complexes are bound by pure van der Waals attractions, which is known to be missing in B3LYP. We thus selected the hydrogen bond systems only. For each system, we keep OBS and PBS to be the same and tested three different basis sets, i.e., aug-cc-pV(D, T, and Q)Z. (See Table IV.) It is clear that the same basis set convergence has

TABLE IV. Tests on selected noncovalent complexes from the A24 data set.[41] Coordinates and the CCSD(T)/CBS interaction energies are all from the same reference. ΔE_{bind}, ΔE_{frz}, and ϵ_ρ are from this work. For each system, three results are presented, which in order are from aug-cc-pV(D, T, and Q)Z basis sets, respectively, for both OBS and PBS. All energy values are in kcal/mol.

System	CCSD(T)/CBS	ΔE_{bind}	ΔE_{frz}	ϵ_ρ
Water···ammonia	−6.493	−5.96/−6.04/−6.05	−3.88/−3.94/−3.96	0.0188/0.0084/0.0033
Water dimer	−5.006	−4.43/−4.49/−4.53	−3.06/−3.10/−3.14	0.0156/0.0088/0.0040
HCN dimer	−4.745	−4.14/−4.19/−4.20	−3.08/−3.10/−3.11	0.0060/0.0033/0.0014
HF dimer	−4.581	−4.29/−4.34/−4.41	−2.74/−2.77/−2.84	0.0142/0.0052/0.0025
Ammonia dimer	−3.137	−2.13/−2.20/−2.21	−1.80/−1.86/−1.87	0.0153/0.0072/0.0021
Formaldehyde dimer	−4.554	−3.05/−3.05/−3.08	−2.01/−1.98/−2.00	0.0259/0.0104/0.0041

been consistently achieved in all systems for both ΔE_{bind} and ΔE_{frz}, even though ϵ_ρ varies.

IV. FROZEN DENSITY ENERGY FOR INTRAMOLECULAR INTERACTIONS AND THE TORSIONAL POTENTIAL OF ETHANE

DEDA is initially developed for intermolecular interactions, and the frozen density energy is the critical intermediate state that allows us to infer the electrostatics and the Pauli repulsions. These two terms together can also be regarded as steric (or nonbonded) effects. The steric effects are important in not only *inter*-molecular interactions, but also *intra*-molecular interactions, a noticeable example being the internal rotation around a single bond, such as that in the ethane molecule.

There are two common ethane conformations: eclipsed and staggered, with the former being the least stable and the latter the most. Their energy difference presents a rotational barrier whose origin has been the subject of too many investigations to be enumerated here. The simple and intuitive explanation of steric effects are often accepted. However, a variety of recently-developed, quantitative, energy decomposition analyses bring diverging viewpoints on the significance of steric[42–44] versus hyperconjugation[45,46] effects. Being mindful of the fact that no single EDA approach can present an unambiguous answer, we nonetheless put DEDA to the test with this classic problem. Part of the reason is that earlier criticisms on different EDA methods for being either nonvariational[43] or for using nonorthogonal orbitals[46] do not apply to DEDA; that is to say, the frozen density energy in DEDA is both variational and does not use nonorthogonal MOs. We are thus motivated to find out whether the frozen density energy can differentiate steric effects from hyperconjugation when bonded interaction is held constant. Our frozen density for either ethane conformation is constructed in the same way as for intermolecular interactions, i.e., sum of methyl fragment densities. We will show that such a choice can indeed provide meaningful results. Alternatively, one may suggest to rigidly rotate the density of one conformation to form the frozen density of other conformations. However, such an approach would require us to divide the total electron density into two parts first: one to be fixed and the other to rotate. Because dividing a molecule into atoms still has ambiguities, we choose not to take this approach in this work.

In Secs. IV A and IV B, we will first compare the results from regular DFT calculations and the frozen density energy at the optimized conformation geometries. We will then focus on the torsion by only changing the dihedral angle while keeping other geometry parameters fixed. The energy differences among ethane conformations represent the torsional potential.

A. Results for optimized geometries

We optimize the geometries for the staggered and eclipsed conformations of ethane at the B3LYP/aug-cc-pVQZ level with Q-Chem.[47] Details of the optimal geometries are summarized on the left side of Table V. The most important structural difference between the optimized staggered and eclipsed conformers, other than the dihedral angle, is the C-C bond length, with the staggered conformer shorter by more than 0.01 Å. In addition, the bond angles within methyl groups are also slightly different, which means the fragment energy and density will be slightly different, too (vide infra). The energy difference between the eclipsed and staggered conformers is 2.64 kcal/mol (4.21 mhartree). Single point calculations using B3LYP and aug-cc-pVTZ orbitals basis set gives nearly identical total energy difference (2.61 kcal/mol), therefore, the B3LYP bonding energy has

TABLE V. Comparison of two ethane conformations. On the left are structures optimized at B3LYP/aug-cc-pVQZ level. Bond lengths are in Å; angles in degree. For the dihedral angle HCCH, only the smallest value is reported. All other structural parameters can be obtained from symmetry. The right half of the table lists various energies (in hartree unless specified) from frozen density calculations using the OBS/PBS combination of aug-cc-pVTZ/aug-cc-pVTZ.

Conformer	Symmetry	$\angle_{\text{HCCH}}$	R_{CC}	R_{CH}	$\angle_{\text{HCH}}$	E_{tot}	E_{frz}	E_{frag}	ϵ_ρ
Staggered	D_{3d}	60.00	1.527	1.090	107.51	−79.864717	−79.823163	−79.689391	0.0262
Eclipsed	D_{3h}	0.00	1.541	1.089	107.05	−79.860564	−79.820508	−79.687707	0.0280
E(eclipsed) − E(staggered) (kcal/mol)						2.61	1.67	1.06	

converged at aug-cc-pVTZ level. Our subsequent calculations are then performed with aug-cc-pVTZ basis set.

We next examine the frozen density energy results at the optimized geometries. We have used aug-cc-pVTZ as the orbitals basis set and aug-cc-pVTZ as the potential basis set. Geometries of the fragments are kept as they are in the molecule. Although each fragment is a radical and should be calculated with unrestricted Kohn-Sham method, we use the total density from each fragment and their simple sum to build the frozen density, the same as for intermolecular interactions. All fragment calculations are done with the basis set of the whole molecule, i.e., BSSE corrected. Results are summarized in the right half of Table V. First thing we notice is that the density error (ϵ_ρ) is comparable to those for neon dimer at $R = 3$ bohrs with the same combination of basis sets, indicating the frozen density energy is near the basis set limit.

We also find that for a given conformation, the frozen density energy already absorbs the majority of the bonding energy. Quantitatively, in both conformations $E_{\text{frz}} - E_{\text{frag}}$ accounts for over 75% of $E_{\text{tot}} - E_{\text{frag}}$, which for the staggered and eclipsed is 110 and 108 kcal/mol, respectively. The chemical picture of a single bond is the pairing of two unpaired electrons, one spin up and one spin down. It leads to accumulation of electron density in the bonding region without violating the Pauli exclusive principle, in contrast to the case when two neon atoms are brought together. Because the frozen density calculation is done for closed-shell ethane, the electron pairing is implicitly accounted for. Being the sum of fragment electron densities, the frozen density also has an accumulation of electron density in the bonding region. Therefore, it is not surprising to see the frozen density energy actually displays the main bonding character. Nonetheless, there is still a sizable energy drop from E_{frz} to E_{tot} (26 and 25 kcal/mol, respectively), indicating that density relaxation also contributes significantly to the bonding. For intermolecular interactions, such relaxation is attributed to polarization and charge transfer. For intramolecular interactions, there is possible additional change in the bonding characters, i.e., due to conjugation or hyperconjugation.

Now let us compare eclipsed and staggered conformation. At optimal geometries, the staggered conformation is lower in energy by 2.61 kcal/mol. If we look at the difference between the two conformations more closely, we see that they differ at the fragment level already. That is to say, the staggered conformation allows its methyl groups to be more relaxed, and their energies are lower by 1.06 kcal/mol than those from the eclipsed conformation. The frozen density energy built from these fragments increases the difference by about 0.6, bringing it to 1.67 kcal/mol. It thus seems that the interactions at the frozen density level do not contribute significantly to the rotational barrier. However, such comparison is rather compounded because not only the fragments are slightly different in these two conformations, the C-C bond length also differs in optimized conformations. The staggered conformation has a shorter C-C distance than the eclipsed, suggesting a stronger bond. The frozen density energy calculated at different bond lengths includes the difference in both the strength of bonded interactions and nonbonded interactions. To gain further insight into the steric effects, we should compare conformations at fixed bond lengths and bond angles. This is based on the following premises that are consistent with conventional bonding picture. First, the electron pairing in the frozen density is only responsible for the carbon-carbon single bond. Any characters beyond single bond will result in density relaxation. Second, the interaction within a single bond presents no rotational barrier. Therefore, if we want to separate the steric effects from hyperconjugation, the frozen density energy difference for conformations at fixed bond lengths and bond angles reflects fully the steric effects, while the difference beyond the frozen density energy accounts for the hyperconjugation. It should be clear by now that by steric effects we mean the part of frozen density interactions due to full electrostatics and the Pauli repulsions between electron pairs from different fragments.

B. The torsional potential profile

The torsional potential is defined solely by the change of the dihedral angle with all other geometric parameters fixed. For this purpose, it is sufficient to consider only the energy changes with the torsion. Because the staggered conformation has the lowest energy, we use it as the zero reference point for all energies. Therefore, with energy values at 60° H-C-C-H angle all set to be zero, we then probe the energy changes at other angles between 0° and 60° in 10° increment. We do this internal rotation at both the optimized staggered and eclipsed conformations; that is, at two different carbon-carbon bond lengths and slightly different methyl geometries. We compare the regular DFT energies (ΔE_{total}) and the frozen density energies (ΔE_{frz}). We further decompose ΔE_{frz} into electrostatic ΔE_{es} and Pauli repulsion ΔE_{rep} contributions, where the electrostatic energy includes the classical Coulomb interactions among nuclei and the frozen electron density, and ΔE_{rep} is the difference between ΔE_{frz} and ΔE_{es}. Our results are listed in Table VI and plotted in Fig. 3.

The figure clearly shows that the rotational profile of the frozen density energy nearly overlaps with that of the total energy, suggesting steric effects be the dominant contributor to the rotational hindrance. In fact, ΔE_{frz} has a slightly higher barrier than ΔE_{total}, meaning that density relaxation due to polarization and hyperconjugation actually lowers the barrier, but the effect is rather small (less than 0.4 kcal/mol). ΔE_{total} shows that rotation at the optimal staggered geometry

TABLE VI. Energy changes (kcal/mol) when rotating ethane from the staggered conformation (60°) to the eclipsed conformation (0°). On left/right, the rotation is at the optimized staggered/eclipsed geometry as in Table V.

	Opt. staggered geom.				Opt. eclipsed geom.			
$\angle_{\text{HCCH}}$	ΔE_{total}	ΔE_{frz}	ΔE_{es}	ΔE_{rep}	ΔE_{total}	ΔE_{frz}	ΔE_{es}	ΔE_{rep}
0°	2.73	3.12	−4.19	7.30	2.49	2.63	−4.12	6.75
10°	2.54	2.90	−3.97	6.87	2.32	2.45	−3.90	6.34
20°	2.04	2.32	−3.30	5.62	1.86	1.94	−3.23	5.17
30°	1.35	1.53	−2.25	3.78	1.23	1.26	−2.19	3.46
40°	0.67	0.76	−1.13	1.88	0.61	0.61	−1.10	1.71
50°	0.18	0.20	−0.30	0.50	0.16	0.16	−0.29	0.45
60°	0.00	0.00	0.00	0.00	0.00	0.00	0.00	0.00

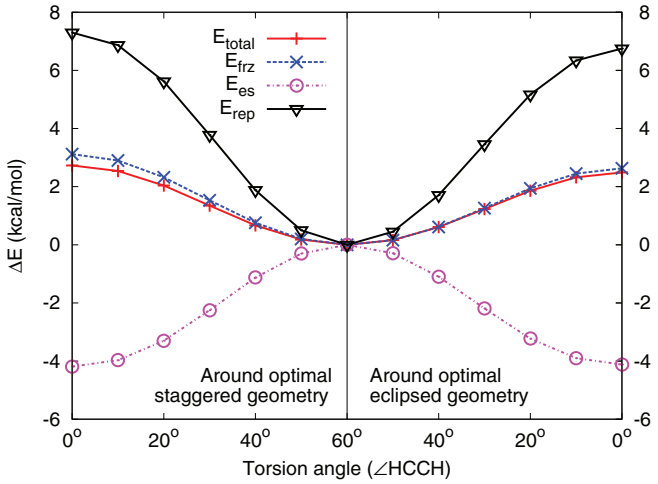

FIG. 3. Rotational profiles of ethane. Points are from Table VI, while lines are used to guide the eye.

has a higher barrier (by 0.24 kcal/mol) than at the eclipsed geometry, which is not surprising because the staggered conformation is the most stable one. Interestingly, ΔE_{frz} further increases this barrier height difference by about 0.25 kcal/mol, but this is not surprising either because of the shorter C-C bond length in the staggered geometry. The idea that steric effects increase when fragments are closer becomes clearer when the components of ΔE_{frz} are examined. While the electrostatic profile is almost the same at either the optimal staggered or eclipsed geometry, the repulsion term has a higher barrier at the staggered geometry as the result of a shorter bond length. Although we do not present the numbers, we can also look into the electrostatics in details. At the eclipsed conformation, even though the electron-electron and nuclei-nuclei repulsions both increase, the effect is more than offset by the increase of electron-nuclear attraction, leading to a net effect of lowering the electrostatic energy from the staggered to the eclipsed conformation. However, the electrostatic stabilization is not sufficient to overcome the increased repulsion at the eclipsed conformation. This trend of ΔE_{es} and ΔE_{rep} has been discussed before,[42] though a different definition of repulsion term is used in that work. Therefore, our DEDA of the torsional potential gives results that are consistent with the view that steric effects cause the rotational barrier height. However, we stress again that this picture is only clear when bond lengths and bond angles are all fixed. Comparing the conformations at their own optimized geometries has no conclusive answer.

V. CONCLUSION

We have elaborated on the variational nature of the frozen density energy as calculated by the Wu-Yang method for constrained search in DFT. After careful analysis of the results for neon dimer, we find that when the same basis set is used for the expansions of the orbitals as well as the potential, a balance of errors leads to a stable frozen density energy. This result justifies our previous studies using the frozen density energy as a critical intermediate state for energy decomposition analysis. More specifically, we find the combination of aug-cc-pVTZ/aug-cc-pVTZ to give a result that is closest to the orbital basis set limit. While our density-based energy decomposition analysis was developed for intermolecular interactions, we explore in this work its utility in analyzing the torsional potential in ethane. We propose that the rotational barrier around a single bond can be understood from the frozen density energy differences, supporting the idea that steric effects are the main force behind the hindrance. Furthermore, we show that the full torsional potential can be almost fully reproduced with the frozen density energy torsional potential, which suggests the combination of electrostatics and Pauli repulsions may be sufficient to model such torsion potentials as in nonconjugated systems. We are currently testing this idea, whose results can be potentially useful for force field development of torsion parameters, extending our early work on electrostatics and van der Waals interactions.[20,21]

ACKNOWLEDGMENTS

Research carried out at the Center for Functional Nanomaterials, Brookhaven National Laboratory is supported by the U.S. Department of Energy, Office of Basic Energy Sciences, under Contract No. DE-AC02-98CH10886.

[1] Q. Wu, P. W. Ayers, and Y. Zhang, J. Chem. Phys. **131**, 164112 (2009).
[2] Y. Mo, J. Gao, and S. D. Peyerimhoff, J. Chem. Phys. **112**, 5530 (2000).
[3] Y. Mo, L. Song, and Y. Lin, J. Phys. Chem. A **111**, 8291 (2007).
[4] K. Kitaura and K. Morokuma, Int. J. Quantum Chem. **10**, 325 (1976).
[5] T. Ziegler and A. Rauk, Theor. Chim. Acta **46**, 1 (1977).
[6] F. M. Bickelhaupt and E. J. Baerends, in *Reviews in Computational Chemistry* (John Wiley & Sons, Inc., Hoboken, NJ, USA, 2000), Vol. 15, pp. 1–86.
[7] W. J. Stevens and W. H. Fink, Chem. Phys. Lett. **139**, 15 (1987).
[8] R. F. Frey and E. R. Davidson, J. Chem. Phys. **90**, 5555 (1989).
[9] P. S. Bagus and F. Illas, J. Chem. Phys. **96**, 8962 (1992).
[10] E. D. Glendening and A. Streitwieser, J. Chem. Phys. **100**, 2900 (1994).
[11] P. Reinhardt, J. P. Piquemal, and A. Savin, J. Chem. Theory Comput. **4**, 2020 (2008).
[12] M. P. Mitoraj, A. Michalak, and T. Ziegler, J. Chem. Theory Comput. **5**, 962 (2009).
[13] P. Su and H. Li, J. Chem. Phys. **131**, 014102 (2009).
[14] P. Su, Z. Jiang, Z. Chen, and W. Wu, J. Phys. Chem. A **118**, 2531 (2014).
[15] Y. Mo, P. Bao, and J. Gao, Phys. Chem. Chem. Phys. **13**, 6760 (2011).
[16] S. N. Steinmann, C. Corminboeuf, W. Wu, and Y. Mo, J. Phys. Chem. A **115**, 5467 (2011).
[17] R. Z. Khaliullin, E. A. Cobar, R. C. Lochan, A. T. Bell, and M. Head-Gordon, J. Phys. Chem. A **111**, 8753 (2007).
[18] P. R. Horn, E. J. Sundstrom, T. A. Baker, and M. Head-Gordon, J. Chem. Phys. **138**, 134119 (2013).
[19] Q. Wu and T. Van Voorhis, Phys. Rev. A **72**, 024502 (2005).
[20] Z. Lu, N. Zhou, Q. Wu, and Y. Zhang, J. Chem. Theory Comput. **7**, 4038 (2011).
[21] N. Zhou, Z. Lu, Q. Wu, and Y. Zhang, J. Chem. Phys. **140**, 214117 (2014).
[22] Q. Wu and W. Yang, J. Chem. Phys. **118**, 2498 (2003).
[23] R. G. Parr and W. Yang, *Density-Functional Theory of Atoms and Molecules* (Oxford University Press, New York, 1989).
[24] M. Levy, Proc. Natl. Acad. Sci. U.S.A. **76**, 6062 (1979).
[25] P. Hohenberg and W. Kohn, Phys. Rev. **136**, B864 (1964).
[26] W. Kohn and L. J. Sham, Phys. Rev. **140**, A1133 (1965).
[27] S. P. Boyd and L. Vandenberghe, *Convex Optimization* (Cambridge University Press, 2004).
[28] D. J. Tozer, V. E. Ingamells, and N. C. Handy, J. Chem. Phys. **105**, 9200 (1996).
[29] S. Fux, C. R. Jacob, J. Neugebauer, L. Visscher, and M. Reiher, J. Chem. Phys. **132**, 164101 (2010).
[30] A. D. Becke, Phys. Rev. A **38**, 3098 (1988).
[31] C. Lee, W. Yang, and R. G. Parr, Phys. Rev. B **37**, 785 (1988).
[32] A. D. Becke, J. Chem. Phys. **98**, 5648 (1993).

[33]R. A. Kendall, E. Aprà, D. E. Bernholdt, E. J. Bylaska, M. Dupuis, G. I. Fann, R. J. Harrison, J. Ju, J. A. Nichols, J. Nieplocha *et al.*, Comput. Phys. Commun. **128**, 260 (2000).
[34]T. H. Dunning, J. Chem. Phys. **90**, 1007 (1989).
[35]R. A. Kendall, T. H. Dunning, Jr., and R. J. Harrison, J. Chem. Phys. **96**, 6796 (1992).
[36]J. E. Harriman, Phys. Rev. A **27**, 632 (1983).
[37]J. E. Harriman, Phys. Rev. A **34**, 29 (1986).
[38]S. F. Boys and F. Bernardi, Mol. Phys. **19**, 553 (1970).
[39]A. Görling, A. Heßelmann, M. Jones, and M. Levy, J. Chem. Phys. **128**, 104104 (2008).
[40]D. E. Hoch and J. E. Harriman, J. Chem. Phys. **102**, 9590 (1995).
[41]J. Řezáč and P. Hobza, J. Chem. Theory Comput. **9**, 2151 (2013).
[42]F. M. Bickelhaupt and E. J. Baerends, Angew. Chem. Int. Ed. **42**, 4183 (2003).
[43]Y. Mo and J. Gao, Acc. Chem. Res. **40**, 113 (2007).
[44]S. Liu and N. Govind, J. Phys. Chem. A **112**, 6690 (2008).
[45]V. Pophristic and L. Goodman, Nature (London) **411**, 565 (2001).
[46]F. Weinhold, Angew. Chem. Int. Ed. **42**, 4188 (2003).
[47]Y. Shao, L. Fusti-Molnar, Y. Jung, J. Kussmann, C. Ochsenfeld, S. T. Brown, A. T. B. Gilbert, L. V. Slipchenko, S. V. Levchenko, D. P. O'Neill *et al.*, Phys. Chem. Chem. Phys **8**, 3172 (2006).